Article

Synchronized, Continuous-Flow Zone Electrophoresis

Dawid R. Zalewski, Dietrich Kohlheyer, Stefan Schlautmann, and Han J. G. E. Gardeniers

Anal. Chem., **2008**, 80 (16), 6228-6234 • DOI: 10.1021/ac800567n • Publication Date (Web): 12 July 2008

Anal. Chem. **2008,** *80,* 6228–6234

Synchronized, Continuous-Flow Zone Electrophoresis

Dawid R. Zalewski,* Dietrich Kohlheyer, Stefan Schlautmann, and Han J. G. E. Gardeniers

MESA+ Institute for Nanotechnology, University of Twente, P.O. Box 217, 7500AE Enschede, The Netherlands

A new method for performing continuous electrophoretic separation of complex mixtures in microscale devices is proposed. Unlike in free-flow electrophoresis devices, no mechanical pumping is required—both fluid transport and separation are driven electrokinetically. This gives the method great potential for on-a-chip integration in multistep analytical systems. The method enables us to collect fractionated sample and tensfold purification is possible. The model of the operation is presented and a detailed description of the optimal conditions for performing purification is given. The chip devices with 10-μm-deep separation chamber of 1.5 mm $\times$ 4 mm in size were fabricated in glass. A standard microchip electrophoresis setup was used. Continuous separation of rhodamine B, rhodamine 6G, and fluorescein was accomplished. Purification was demonstrated on a mixture containing rhodamine B and fluorescein, and the recovery of both fractions was achieved. The results show the feasibility of the method.

The separation of multicomponent samples plays an important role in (bio)analytical sciences. Many traditional separation methods have been downscaled to microfluidic format, and numerous applications of such miniaturized systems have been shown.[1,2] Continuous separation techniques offer clear advantages over batch-type systems[3] and various microscale, continuous separation devices have been demonstrated,[4–10] including both scaled-down counterparts of traditional instruments and systems based on newly discovered phenomena. Among them, free-flow zone electrophoresis[11] and free-flow isoelectric focusing[12] have recently gained attention, and several groups reported their progress with these methods.[13–17] Yet, despite their development, the free-flow electrophoretic techniques share a weakness—both mechanical pumping and high-voltage supply are required for their operation. Usually additional time is required to perform preparation steps specific to a hydraulic setup (e.g., cleaning of external fluidic system, making pressure-resistant connections). Moreover the presence of the pressure-driven flow within the device may lead to difficulties during the on-a-chip integration with follow-up electrokinetic postprocessing (e.g., orthogonal separation methods).

In this paper, we demonstrate a new method of continuous sample separation by zone electrophoresis. Unlike in the free-flow electrophoresis, no mechanical pumping is required; the device relies on electrokinetic flow control only, greatly reducing its complexity. The separation is performed in a microfluidic rectangular chamber, having three inlets on one side and three outlets on the opposite side. A constant-velocity flow is forced in the chamber by applying high voltages (up to 1 kV) to the inlets and the outlets. A sample is injected into the chamber through the middle inlet channel and is electrokinetically focused[18] to form a narrow stream, sandwiched between two sheath streams containing a buffer solution only. The lateral position of the sample stream at the chamber entrance is varied over time in a predefined way, similarly to the continuous electrophoresis in rectangular channels method.[19,20] This, combined with an axial electric field, produces a wavelike sample stream pattern in the chamber. Due to the differences in apparent mobilities of the sample components, a separation of the sample in the axial direction occurs. This is observed as traveling waves with different periods, each wave belonging to one component. By employing synchronized switching of the voltages applied to the outlet channels, as explained in the Experimental Section, one of the separated components can be collected into the middle outlet channel. This new method, called by us a synchronized, continuous-flow zone electrophoresis, has a number of potential applications as a prefractionation or purification method in multidimensional separation systems. It also can be applied in integrated chemical microreactors[21] for monitoring reaction rate or removal of unwanted products. Its great

* To whom correspondence should be addressed. E-mail: D.R.Zalewski@utwente.nl. Phone: +31534892594.

(1) Vilkner, T.; Janasek, D.; Manz, A. *Anal. Chem.* **2004**, *76*, 3373–3385.
(2) Dittrich, P. S.; Tachikawa, K.; Manz, A. *Anal. Chem.* **2006**, *78*, 3887–3907.
(3) Pamme, N. *Lab Chip* **2007**, *7*, 1644–1659.
(4) Han, J.; Craighead, H. G. *Science* **2000**, *288*, 1026–1029.
(5) Pamme, N.; Manz, A. *Anal. Chem.* **2004**, *76*, 7250–7256.
(6) Janasek, D.; Schilling, M.; Franzke, J.; Manz, A. *Anal. Chem.* **2006**, *78*, 3815–3819.
(7) Song, Y. A.; Hsu, S.; Stevens, A. L.; Han, J. Y. *Anal. Chem.* **2006**, *78*, 3528–3536.
(8) Choi, S.; Park, J. K. *Lab Chip* **2007**, *7*, 890–897.
(9) Fu, J. P.; Schoch, R. B.; Stevens, A. L.; Tannenbaum, S. R.; Han, J. Y. *Nat. Nanotechnol.* **2007**, *2*, 121–128.
(10) Petersson, F.; Aberg, L.; Sward-Nilsson, A. M.; Laurell, T. *Anal. Chem.* **2007**, *79*, 5117–5123.
(11) Raymond, D. E.; Manz, A.; Widmer, H. M. *Anal. Chem.* **1994**, *66*, 2858–2865.
(12) Xu, Y.; Zhang, C. X.; Janasek, D.; Manz, A. *Lab Chip* **2003**, *3*, 224–227.
(13) Albrecht, J. W.; Jensen, K. F. *Electrophoresis* **2006**, *27*, 4960–4969.
(14) de Jesus, D. P.; Blanes, L.; do Lago, C. L. *Electrophoresis* **2006**, *27*, 4935–4942.
(15) Fonslow, B. R.; Bowser, M. T. *Anal. Chem.* **2006**, *78*, 8236–8244.
(16) Albrecht, J. W.; El-Ali, J.; Jensen, K. F. *Anal. Chem.* **2007**, *79*, 9364–9371.
(17) Kohlheyer, D.; Eijkel, J. C. T.; Schlautmann, S.; van den Berg, A.; Schasfoort, R. B. M. *Anal. Chem.* **2007**, *79*, 8190–8198.
(18) Jacobson, S. C.; Ramsey, J. M. *Anal. Chem.* **1997**, *69*, 3212–3217.
(19) Mesaros, J. M.; Luo, G.; Roeraade, J.; Ewing, A. G. *Anal. Chem.* **1993**, *65*, 3313–3319.
(20) Mesaros, J. M.; Ewing, A. G. *J. Microcolumn Sep.* **1994**, *6*, 483–494.
(21) Belder, D.; Ludwig, M.; Wang, L. W.; Reetz, M. T. *Angew. Chem.,Int. Ed.* **2006**, *45*, 2463–2466.

10.1021/ac800567n CCC: $40.75
Published on Web 07/12/2008

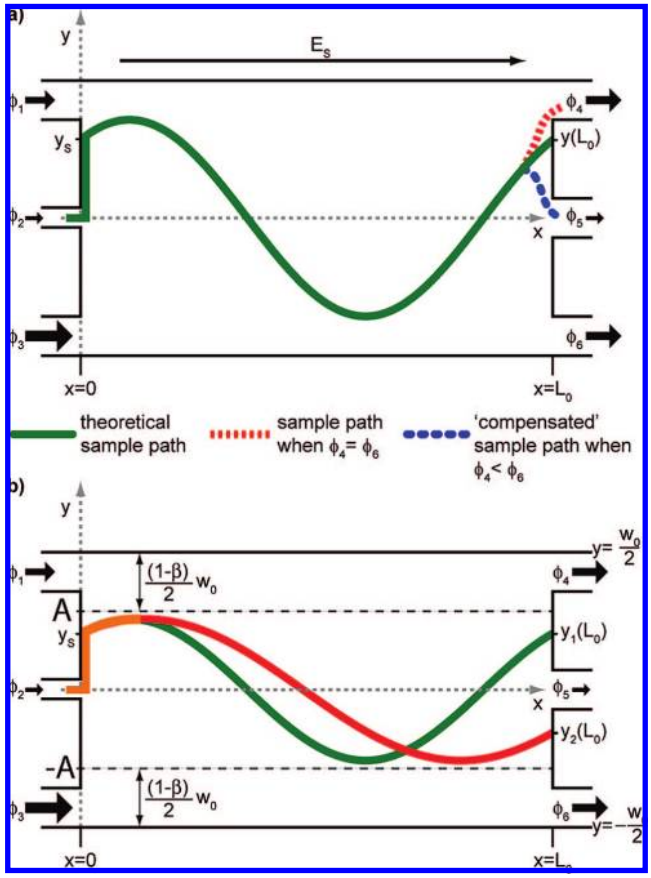

Figure 1. Principle of synchronized, continuous-flow zone electrophoresis: (a) altering outlet fluxes for continuous sample collection; (b) two-components case.

advantage is a lack of pressure-driven flow, which simplifies interfacing with other purely electrokinetic systems.

EXPERIMENTAL SECTION

Theory of Operation. To explain the principle of the method, we refer to Figure 1. The basic device assembly consists of a microfluidic laminar-flow chamber with three inlets and three outlets. The flow within the device is induced electrokinetically and controlled by adjusting high voltages applied to the inlets and the outlets in an appropriate manner. The middle inlet is used for introducing a sample into the chamber, whereas the two outer inlets provide sheath streams for manipulating the position and the width of the sample stream by electrokinetic steering.[22] The presence of the transverse electric field in the vicinity of the entrance and the exit of the chamber is neglected. The electric field throughout the separation chamber E_S is assumed to be uniform; also, the flow within the chamber is considered to be a fully developed plug flow. During the operation, the starting position of the sample stream y_S is varied periodically according to

$$y_s(t) = A \sin(\omega t) \tag{1}$$

where A is the amplitude and ω is the angular frequency of the oscillation. This, combined with the flow in the axial direction (x), driven by the electric field E_S, results in a wavelike sample stream path, which takes the theoretical form

$$y(x,t) = -A \sin\left(\omega\left(\frac{x}{\mu_s E_s} - t\right)\right) \tag{2}$$

Here μ_S denotes the apparent mobility of the sample. The real shape of this curve near the chamber exit is determined by the flow rates of the outlet streams. If, in the case of the sample stream pattern shown in Figure 1a, the sheath outlet fluxes are equal and much greater than the middle outlet flux, the sample stream will be bent toward the upper outlet. However, it is possible to adjust the steering voltages in such a way that the sample stream will exit through the middle outlet. To achieve this, a switching pattern similar to at the inlet of the chamber must be employed at the outlet. In the case presented in Figure 1a, increasing the flux ϕ_6, while lowering the flux ϕ_4 and keeping the middle outlet flux at the level of the sample inlet flux, should result in guiding the sample stream into the middle outlet.

If a multicomponent mixture is used as a sample, and the components differ in apparent mobilities, additional sample waves, with shapes adhering to (2) will be present in the chamber (Figure 1b). A steering scheme, where the outlet fluxes are continuously altered to guide one of the exiting component streams into the middle outlet channel, results in the collection of its purified fraction. We refer to this effect as synchronized, continuous-flow zone electrophoresis (SCFZE).

Synchronized Steering. For controlling the separation process, the running electrolyte properties (conductivity σ_0 and mobility μ_0), as well as exact dimensions of the chamber and inlet and outlet channels must be known. Prior to operation, the following values should be also provided: the electric field strength E_S, the sample stream width given as a fraction of the chamber width α, the sample confinement coefficient β (i.e., a fraction of the chamber width, where a sample wave is present: see Figure 1b), the angular frequency ω at which the sample stream starting position varies according to (1), and the apparent mobility of the component to be collected μ_S, which is the sum of the electrophoretic and electroosmotic mobilities. The total flux through the chamber is then given as

$$\varphi_0 = \mu_0 E_s S_0 \tag{3}$$

where S_0 is the cross-sectional area of the chamber. Consequently, the fluxes through the inlets and outlets, as functions of time, can be derived:

$$\begin{aligned}
\varphi_2(t) &= \varphi_5(t) = \alpha\varphi_0 \\
\varphi_1(t) &= \varphi_{\min} + \frac{A - y_i(0,t)}{2A}(\beta - \alpha)\varphi_0 \\
\varphi_3(t) &= \varphi_{\min} + \frac{A + y_i(0,t)}{2A}(\beta - \alpha)\varphi_0 \\
\varphi_4(t) &= \varphi_{\min} + \frac{A - y_i(L_0,t)}{2A}(\beta - \alpha)\varphi_0 \\
\varphi_6(t) &= \varphi_{\min} + \frac{A + y_i(L_0,t)}{2A}(\beta - \alpha)\varphi_0
\end{aligned} \tag{4}$$

The function $y_i(x,t)$ defined in (2) is evaluated for the mobility of a collected component, and L_0 denotes the length of the chamber. The amplitude A of the wave equals

(22) Besselink, G. A. J.; Vulto, P.; Lammertink, R. G. H.; Schlautmann, S.; van den Berg, A.; Olthuis, W.; Engbers, G. H. M.; Schasfoort, R. B. M. *Electrophoresis* **2004**, *25*, 3705–3711.

$$A = \frac{\beta - \alpha}{2} w_0 \quad (5)$$

where w_0 is the width of the chamber. The minimum sheath stream flux ϕ_{min} is derived from the confinement coefficient:

$$\varphi_{min} = \frac{1-\beta}{2} \varphi_0 \quad (6)$$

The electric currents flowing through the inlet and outlet channels can be obtained from the fluxes by using the dependency

$$i_i(t) = \varphi_i(t) \frac{\sigma_0}{\mu_0} \quad (7)$$

Then, the relations between the steering voltages that need to be applied to the channels are derived by using Kirchhoff's laws[23,24] and resistance values of the channels and the chamber evaluated from then known device dimensions. Since the system of equations produced by such analysis in unsolvable, the lowest applied potential (one of the side outlet channels) is assumed to equal zero, which allows evaluating the remaining potentials.

Microchip Fabrication. The chip was manufactured in borosilicate glass, utilizing standard microfabrication techniques.[25] Briefly, two glass plates were used; the top plate contains the fluidic channels as well as reservoir openings. The channels were created by etching in hydrofluoric acid through a patterned Cr/Au mask. The reservoirs openings were fabricated by powder-blasting with Al_2O_3 particles through a patterned polymer photoresist foil. Next, the resting masking material was removed and the wafers were thermally bonded. Finally, the bonded wafer stack was diced into separate chip devices.

Chemicals. All chemicals were purchased from Sigma-Aldrich-Fluka. A 20 mM MES/histidine solution at pH 6.35 was used as a buffer. The two-component sample contained 500 μM rhodamine B, 750 μM fluorescein in a buffer solution. The three-component sample consisted of 100 μM rhodamine B, 50 μM fluorescein, and 100 μM rhodamine 6G in a buffer solution. All fluids contained 3% (v/v) isopropyl alcohol to improve solubility of sample components and 0.05% (w/v) Tween 20 to overcome difficulties with filling the separation chamber. Solutions were filtered through a 0.22-μm membrane filter and degassed for 5 min in a vacuum chamber.

Apparatus and Procedures. The chips were stored in demineralized water. Prior to experiments, they were placed in a custom-made holder and flushed for 5 min with the buffer solution. Then, the buffer in the reservoirs was exchanged and a sample mixture was introduced into the middle inlet reservoir. Following this, the experiments were started immediately. Two computer-controlled, high-voltage power supplies (IBIS B.V., Hengelo, The Netherlands) were used to steer the device. They were controlled by a native Windows application, written in-house, with 40-Hz frequency (i.e., the voltages were updated in 25-ms intervals). The images were captured with a digital color camera ColorViewII (Olympus) mounted to a fluorescence microscope (Olympus IX51) equipped with a mercury lamp and a fluorescent filter sets (XF57, Omega Optical and 11012v2, Chroma Technology). The exposure time for the images was 100 ms unless otherwise stated. Numerical computations were performed in Matlab 7 software package using built-in numerical integration functions and a self-written trapezoidal rule integration function.

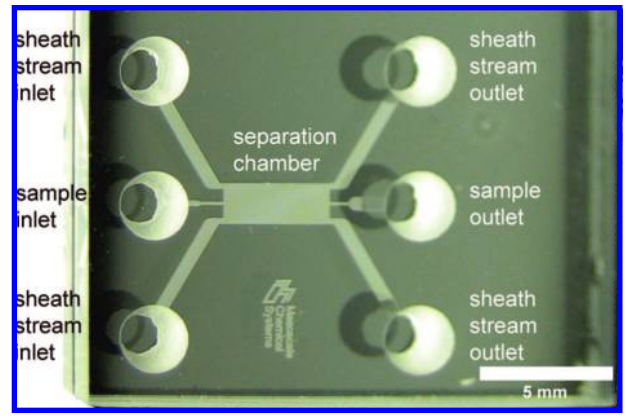

Figure 2. A photograph of the fabricated chip devices.

Table 1. List of Parameters Used during the Separation and Purification Experiments

no.	E_S V·cm^{-1}	m^2 μ_S (V·s)$^{-1}$	ω rad·s^{-1}	α	β
separation, 2 components	300	1.97×10^{-8}	π	0.01	0.9
separation, 3 components	350	3.55×10^{-8}	0.5π	0.01	0.8
no synchronization	400	2.35×10^{-8}	0.5π	0.005	0.4
rhodamine B synchronization	400	1.97×10^{-8}	0.5π	0.005	0.4
fluorescein synchronization	400	1.02×10^{-8}	0.5π	0.01	0.4

RESULTS AND DISCUSSION

Chip Devices. A fabricated chip is shown in Figure 2. The chips are 20 mm × 15 mm in size. The etched channels depth is 10 μm. The side inlets and outlets are 500 μm wide and 4300 μm long. Both the sample inlet channel and the sample outlet channel consist of two parts with different dimensions. For the inlet they are as follows: 1200 μm long, 200 μm wide and 900 μm long, 100 μm wide, respectively; and for the outlet, 750 μm long, 100 μm wide and 1350 μm long, 500 μm wide. The separation chamber dimensions are 4000 μm × 1500 μm.

Separation. Table 1 summarizes the parameters values used in the experiments.

The separation tests were performed on both sample mixtures, one containing two components and another three components. Figure 3 shows a sequence of images taken near the chamber entrance during the separation of rhodamine B and fluorescein mixture. The separation of the sample occurs as predicted by the theory. However, the amplitude of the fluorescein wave is lower than the rhodamine wave amplitude. This phenomenon is caused by the difference in the mobilities of the components (rhodamine B is neutral, while fluorescein is negatively charged; thus the net

(23) Ermakov, S. V.; Jacobson, S. C.; Ramsey, J. M. *Anal. Chem.* **2000**, *72*, 3512–3517.
(24) Kohlheyer, D.; Besselink, G. A. J.; Lammertink, R. G. H.; Schlautmann, S.; Unnikrishnan, S.; Schasfoort, R. B. M. *Microfluidics Nanofluidics* **2005**, *1*, 242–248.
(25) Zalewski, D. R.; Schlautmann, S.; Schasfoort, R. B. M.; Gardeniers, J. G. E. *Lab Chip* **2008**, *8*, 801–809.

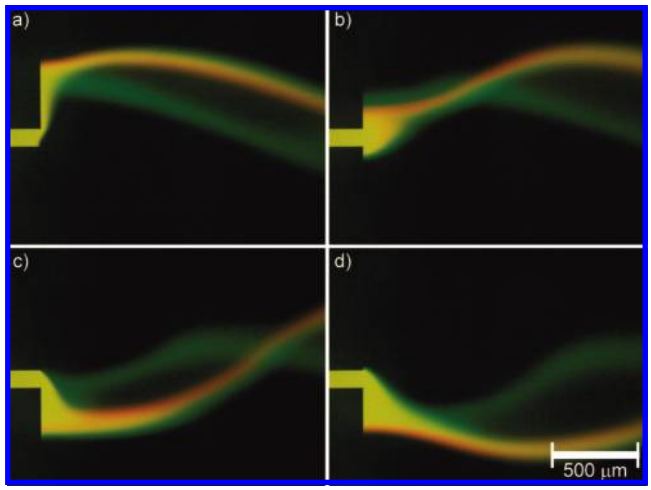

Figure 3. Separation of rhodamine B (red/orange) and fluorescein (green) mixture. The amplitude of the fluorescein wave is visibly smaller than that of rhodamine due to its lower mobility.

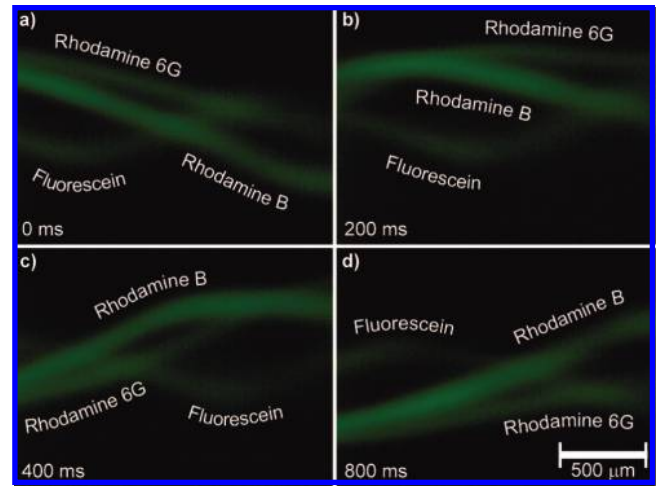

Figure 4. Separated component streams of rhodamine B, rhodamine 6G and fluorescein. The separation between the rhodamine dyes is significantly worse near the wave maximums. (Different color scheme of this image is caused by the use of a different filter set—necessary, due to low dye concentrations).

mobility of rhodamine B is greater than of fluorescein[26]). In fact, to modulate the sample wave properly, the following condition must be valid:

$$\frac{dy_s(t)}{dt} \leq \mu_s E_T \tag{8}$$

where E_T is the transient, transverse electric field, present in a small region near the chamber entrance,[22] which causes the sample stream starting position to move up and down. This effect is not considered in the presented theory of SCFZE, where uniformity of the electric field in the chamber is assumed. Its influence can be avoided by lowering the modulation frequency or the amplitude to obey the condition in eq 8. The visible, relatively large width of the component streams is partially caused by long exposure times that were used due to the equipment limitations.

To test the separation efficiency for species with smaller difference in mobilities, a three-component mixture was used containing fluorescein, rhodamine B, and rhodamine 6G. Figure 4 shows pictures of separated sample streams taken at ~1/3 of the chamber length. The differences in the net mobilities of the components ($|\mu_{rho6G} - \mu_{rhoB}| < |\mu_{rhoB} - \mu_{fluo}|$) result in significant differences in spatial separation between the streams. Moreover, the spacing between the two rhodamine dyes is not evident near the maximums of the waves. This effect is caused both by the diffusion and the shape of the waves and can be minimized by changing the amplitude modulation function (1).

Synchronized Collection and Purification. The demonstration of SCFZE was performed on a sample containing fluorescein and rhodamine B. The values of the mobilities of the components, needed for accurate synchronization, were found experimentally by starting the process with synchronization to the sample mobility $\mu_S = 4.0 \times 10^{-8}$ m^2·(V s)$^{-1}$ and lowering its value in 0.05×10^{-8} m^2·(V s)$^{-1}$ steps. Figure 5a–d show typical paths of the components streams in the chamber exit region, when neither component is synchronized. Both component streams are being swept over the whole width of the chamber. As a result, the components enter all three outlets periodically and no collection of a purified component occurs. Corresponding images of the sample collection channel can be seen in Figure 5 e,f, where similar amount of both components enters the channel and is collected. This is observed as alternating strips of fractions separated by pure buffer volumes. The broadening of the streams in the vicinity of the outlets, most pronounced in Figure 5a, is caused by the electric field distribution present in the electrokinetic guiding scheme[22] and the diffusion of the sample.

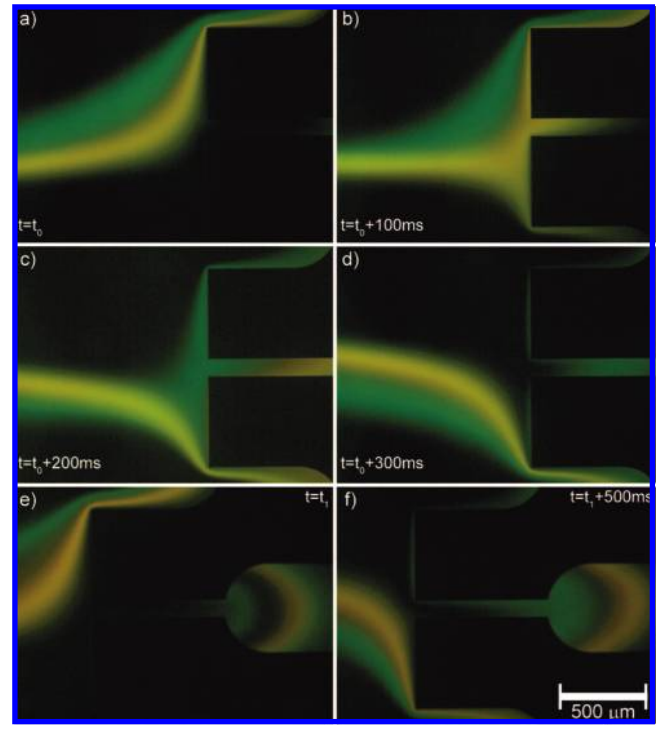

Figure 5. Unsynchronized fractionation of two-component sample. (a–d) Typical component streams; (e, f) collection of both components into the sample outlet channel occurs.

(26) Kohlheyer, D.; Besselink, G. A. J.; Schlautmann, S.; Schasfoort, R. B. M. *Lab Chip* **2006**, *6*, 374–380.

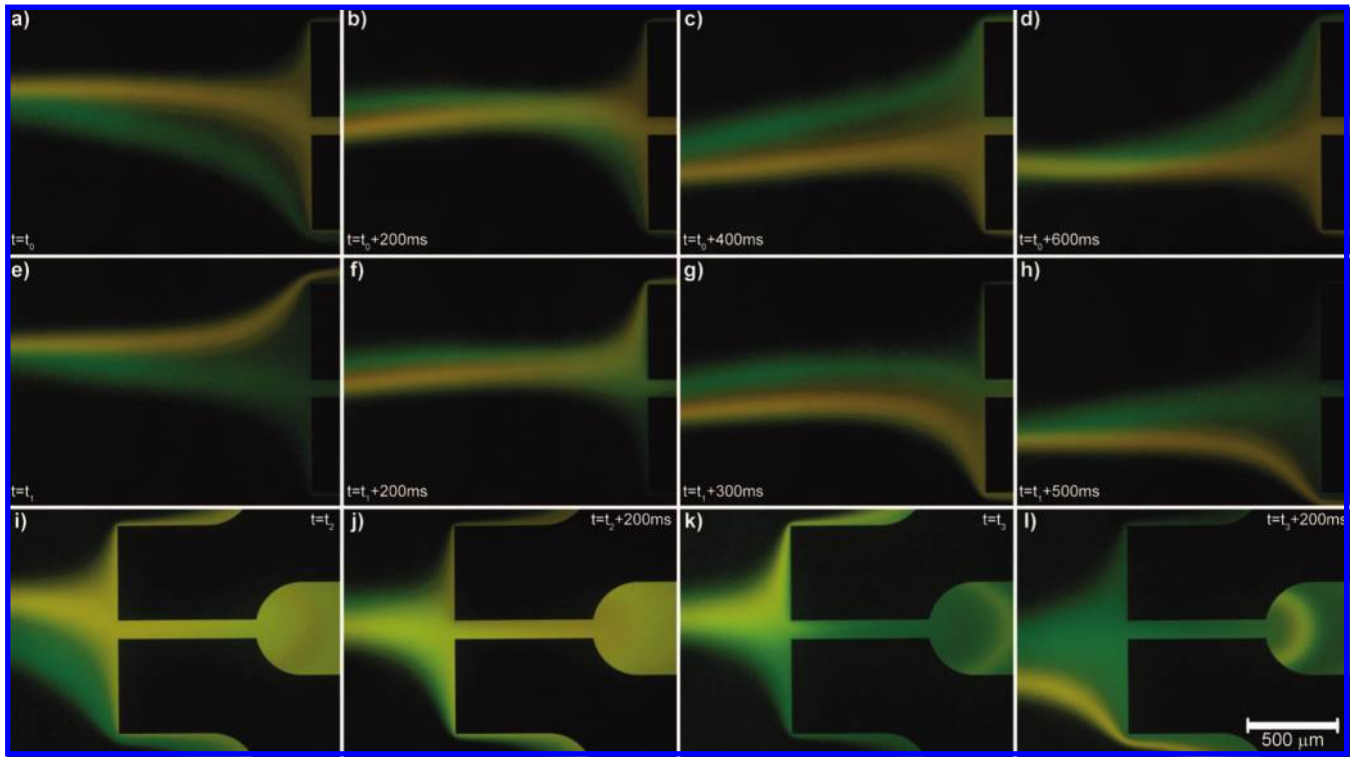

Figure 6. Sequence of images taken during the synchronized fractionation of a rhodamine B, fluorescein mixture: (a−d) collection of rhodamine B; (e−h) collection of fluorescein. Corresponding images of outlet channel for (i, j) rhodamine B collection and (k, l) fluorescein collection.

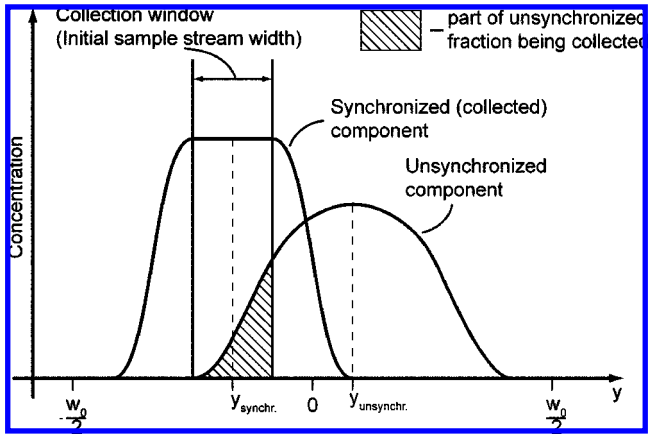

Figure 7. Schematic representation of concentration profiles of two diffusing sample streams at the end of the separation chamber.

The values of the apparent mobilities for which the synchronization was observed were 1.97×10^{-8} m^2·(V s)$^{-1}$ for rhodamine B and 1.02×10^{-8} m^2·(V s)$^{-1}$ for fluorescein. The remaining parameters can be found in Table 1. The image sequence taken during the synchronized collection of rhodamine B is shown in Figure 6a−d. The most distinct difference, as compared to the unsynchronized fractionation case shown in Figure 5, is that the rhodamine fraction stream, despite its original position, now always enters the middle collection channel. This is accomplished by adjusting the magnitudes of the outlet fluxes according to eq 4. The result of this action is observed, near the end of the chamber, as a deflection of the rhodamine stream toward the middle outlet. The remaining fraction (fluorescein) is still being swept over the whole chamber width as in the case of unsynchronized fractionation.

Likewise, the collection of purified fluorescein fraction is shown in Figure 6e−h. Again a characteristic deflection can be seen.

The corresponding images of the sample outlet channel are presented in Figure 6i,j and Figure 6k,l for the synchronized collection of rhodamine B and fluorescein, respectively. The collected fractions are visually pure with an exception for small contamination rings (better visible, due to the used optical filter set characteristics, in the case of fluorescein collection).

The broadening of the collected sample streams, seen in Figure 6, is caused by the electric field distribution, similarly as observed for Figure 5. Despite some sample loss caused by this effect, it is negligible for purification or fractionation purposes.

Contamination. The contamination of a collected component by unsynchronized fractions, as seen in Figure 6, is unavoidable. In principle, the contamination occurs when the lateral positions at the end of the chamber of both, the synchronized and the unsynchronized sample streams are equal:

$$y_s(L_0, t) = y_{us}(L_0, t) \tag{9}$$

where $y(L_0, t)$ is defined by eq 2. When it happens, the unsynchronized sample stream is forced to enter the middle outlet together with the collected component. Equation 9 has two solutions. One of them is given by

$$\frac{1}{\mu_s} - \frac{1}{\mu_{us}} = \frac{2k\pi E_s}{\omega L_0} \qquad k = 0, \pm 1, \pm 2, \ldots \tag{10}$$

This solution is independent of time. It means that, when the mobility of the collected component μ_s and the mobility of the

unsynchronized fraction μ_{us} satisfy the condition given in (10), the streams overlap at any instant of time at the end of the chamber; thus the contamination occurs continuously. Equation 10 can be used to generate, by varying k, a set of mobilities for a given sample mobility μ_s and parameters E_S, ω, and L_0. The fractionation of a mixture, containing components with mobilities belonging to such set, is impossible under the conditions described by the parameters used to generate it. Yet, they can be still fractionated by changing either the separation field E_S or the angular frequency of modulation ω, in such a way, that the condition defined in (10) is not valid.

Another solution can be obtained by solving (9) for time t. It shows that for the samples and the fractionation conditions that do not satisfy (10) the contamination occurs periodically with the frequency

$$f_{cont} = \frac{\omega}{\pi} \tag{11}$$

In the experiments of synchronized fractionation of the rhodamine B/fluorescein mixture, described in this report, $f_{cont} = 0.5$ Hz. The interpretation of eq 11 can be misleading. It shows that lowering the modulation frequency results in less frequent occurrence of the unsynchronized stream entering the sample outlet. However, the initial width of the streams and the lateral diffusion are not considered in eq 9, and thus, in its solutions—the sample streams are assumed to be infinitesimally narrow. As a consequence, f_{cont} does not provide any quantitative information about the contamination level. To assess the amount of contamination, we performed numerical computation.

On the assumption, that the electric field in the chamber E_S is uniform, the concentration function of a sample with the apparent mobility μ_i and the stream path $y_i(x,t)$ defined in eq 2 is given by[27]

$$C_i(x,y,t) = \frac{C_{0,i}}{2}\left[\operatorname{erf}\left(\frac{\frac{\alpha w_0}{2} - y + y_i(x,t)}{2\sqrt{D_i \frac{x}{\mu_i E_s}}}\right) + \operatorname{erf}\left(\frac{\frac{\alpha w_0}{2} + y - y_i(x,t)}{2\sqrt{D_i \frac{x}{\mu_i E_s}}}\right)\right] \tag{12}$$

Figure 7 shows a schematic plot of lateral concentration profiles of two components at the end of the separation chamber ($x = L_0$). The middle point $y_{unsynchr}$ of the unsynchronized component lies outside the collection window. However, due to the diffusion, a part of it is collected together with the synchronized fraction, causing contamination.

For a mixture containing n components, the total collected amount of material of the ith component m_i, during the synchronized collection of the jth component, in the time interval T, can be calculated by solving the double integral

$$m_i = \mu_i E_s \int_T \int_{y_j - 0.5\alpha w_0}^{y_j + 0.5\alpha w_0} C_i(L_0, y, t)\, \mathrm{d}y\, \mathrm{d}t \tag{13}$$

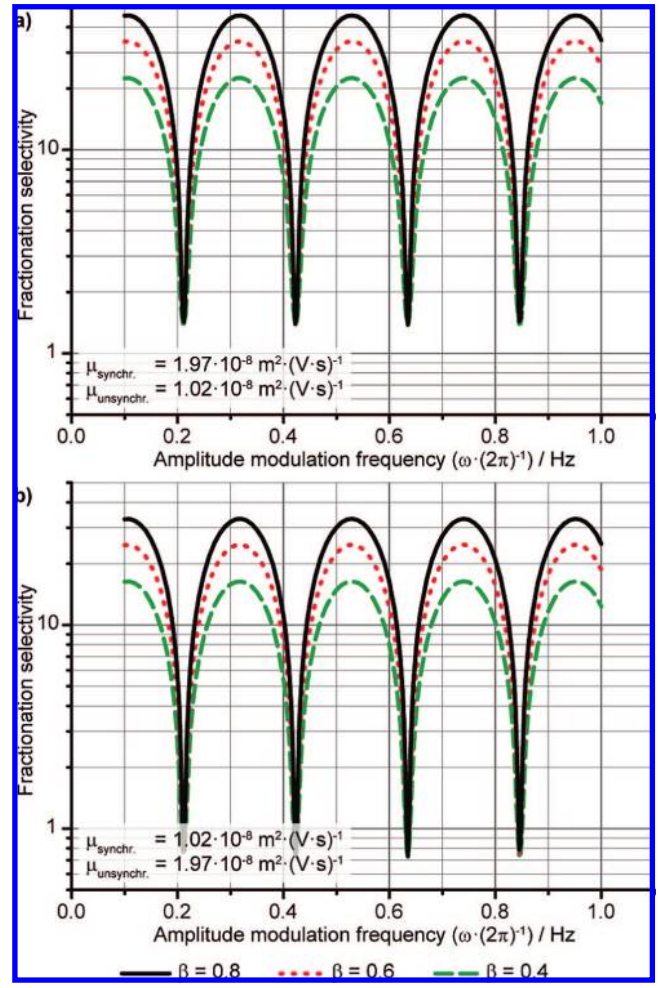

Figure 8. Fractionation selectivity for the synchronized fractionation of a two-component mixture. Selectivity for collection of the component with higher (a) and lower (b) mobility. The selectivity exhibits periodic variations, dependent on the amplitude modulation frequency.

where y_j, present in the integration limits, is the position function (2) of the synchronized component evaluated for $x = L_0$. The numerical computations of the integral (13) were performed for a two-component mixture. The parameters used for the calculations were as follows: the mobilities of the components $\mu_1 = 1.97 \times 10^{-8}$ m^2·(V s)$^{-1}$, $\mu_2 = 1.02 \times 10^{-8}$ m^2·(V s)$^{-1}$, the diffusivities of the components $D_1 = D_2 = 1 \times 10^{-10}$ m^2·s^{-1}, the separation field $E_S = 400$ V·cm^{-1}, and the stream width coefficient $\alpha = 0.01$. The physical dimensions of the chip device described in this article were used. Figure 8 shows the results of the calculations. The fractionation selectivity versus the modulation frequency is plotted, for the collection of the faster (Figure 8a) and the slower (Figure 8b) components. The fractionation selectivity was calculated as

$$S = \frac{M_{us} m_s}{m_{us} M_s} \tag{14}$$

where M_s, M_{us} are the total masses entering the separation chamber of the synchronized and unsynchronized components, respectively, and m_s, m_{us} are the collected masses of the

(27) Crank, J. *The mathematics of diffusion*, 2 ed.; Clarendon Press: Oxford, 1975.

Table 2. Maximum and Minimum Purification Ratios for the Synchronized Fractionation of the Two-Component Mixture, with Component Mobilities $\mu_1 = 1.97 \times 10^{-8}$ $m^2 \cdot (V\ s)^{-1}$ and $\mu_2 = 1.02 \times 10^{-8}$ $m^2 \cdot (V\ s)^{-1}$

	Pur_{max}			Pur_{min}
β	0.4	0.6	0.8	independent
$\mu_{s,} = 1.97 \times 10^{-8}$ $m^2 \cdot (V\ s)^{-1}$	43.51	65.92	88.32	2.66
$\mu_{s,} = 1.02 \times 10^{-8}$ $m^2 \cdot (V\ s)^{-1}$	8.48	12.84	17.20	0.38

synchronized and unsynchronized components. When the selectivity drops below 1, a bigger part of the unsynchronized component flowing through the chamber is collected than of the synchronized component.

As can be seen in Figure 8, the selectivity exhibits periodic variations, and reaches the maximum values for

$$\omega = \frac{(2k+1)\pi\mu_s\mu_{us}E_s}{L_0|\mu_s - \mu_{us}|} \qquad k = 0, 1, 2, \ldots \tag{15}$$

The selectivity values depend not only on the amplitude modulation frequency ω and the sample confinement coefficient β but also on the sample chosen for collection. This effect is caused by the difference in the mobilities of components. The mobility determines not only the flux of a component but also the residence time in the chamber (i.e., the time needed for the sample to travel the distance of the chamber length). Thus, the diffusional dispersion at the end of the chamber of the sample stream of the less mobile component is greater than that of the more mobile component. As a consequence of these phenomena, less material of the slower component is collected per time unit than of the faster component, even if their streams overlap continuously at the collection point (selectivity minimums in Figure 8).

Table 2 summarizes the maximum and minimum values of purification ratios derived for the computed fractionation selectivities. The purification ratio is defined as

$$Pur = \frac{C_s}{C_{us}}\frac{C^*_{us}}{C^*_s} = \frac{\mu_s}{\mu_{us}}s \tag{16}$$

where C is the concentration of the collected component and C^* is its initial concentration. The 10-fold purification can be easily achieved for the tested mixture, and much higher rates are possible by adjusting fractionation parameters.

CONCLUSIONS

Microfluidic, synchronized, continuous-flow zone electrophoresis was successfully demonstrated for the first time. The theoretical model of the method was presented and applied in the experimental setup. The results positively validate the model. Continuous separation and continuous fractionation with collection of the purified components were achieved in the electrokinetic-only microchip device. The theoretical explanation of the influence of the fractionation parameter on the efficiency of the collection process was given, together with the derivation of the optimal values. By choosing appropriate operating parameters, it is possible to perform tens-fold purification by SCFZE. Synchronized, continuous-flow zone electrophoresis can be relatively easily performed by extending standard microchip CE setups. Further improvement of the method is possible, both theoretical and practical by, for example, optimizing the device geometry, changing the amplitude modulation function, and extending the theoretical description to include the effects not considered in the current model. SCFZE has a potential broad application area as a purification or prefractionation tool in integrated separation and analytical systems.

ACKNOWLEDGMENT

The authors gratefully acknowledge Paul Vulto for helpful discussions and Geert A.J. Besselink and Hans de Boer for their experimental and technical support.

Received for review March 19, 2008. Accepted May 28, 2008.

AC800567N